Journal of Solid State Chemistry **156,** 408–414 (2001)
doi:10.1006/jssc.2000.9014, available online at http://www.idealibrary.com on IDEAL®

Influence of Zinc Doping on the Structural and Magnetic Properties of α-Fe_2O_3

Ibrar Ayub,* Frank J. Berry,*,[1] Robert L. Bilsborrow,† Örn Helgason,‡ Roberto C. Mercader,§ Elaine A. Moore,* Silvana J. Stewart,*,§ and Paul G. Wynn*

*Department of Chemistry, The Open University, Walton Hall, Milton Keynes MK7 6AA, United Kingdom; §Departamento de Fisica, Universidad Nacional de La Plata, CC67, 1900 La Plata, Argentina; ‡Science Institute, University of Iceland, Dunhagi 3, 1S-107 Reykjavik, Iceland; and †Daresbury Laboratory, Daresbury, Warrington WA4 4AD, United Kingdom

Received June 14, 2000; in revised form October 5, 2000; accepted October 27, 2000

Zinc-doped α-Fe_2O_3 has been prepared by hydrothermal methods. The zinc K-edge EXAFS and interatomic potential calculations indicate that Zn^{2+} ions substitute for Fe^{3+} ions in the lattice and are accompanied by oxygen vacancies. The ^{57}Fe Mössbauer spectra recorded between 296 and 18 K demonstrate that the Morin transition in α-Fe_2O_3 is completely suppressed within this temperature range by the presence of zinc. The ^{57}Fe Mössbauer spectra recorded *in situ* at temperatures between 300 and 915 K show the material to undergo conversion to the spinel-related $ZnFe_2O_4$ phase in this temperature regime. The results demonstrate that the structural and magnetic properties of zinc-doped α-Fe_2O_3 and its behavior at elevated temperatures are different from those of magnesium-doped α-Fe_2O_3. © 2001 Academic Press

INTRODUCTION

The influence of dopant cations on the electrical, magnetic, and other physical properties of α-Fe_2O_3 has been an area of interest for some time (1–12). The nature of the sites occupied within the corundum-related α-Fe_2O_3 structure has often been the subject of speculation and the influence of dopants on some properties, such as the Morin transition temperature, are not well understood (13).

We have recently reported on the structural characterization by X-ray powder diffraction of materials of the type α-$Fe_{2-x}M_xO_3$ ($M = Sn^{4+}$, Ti^{4+}, Mg^{2+}) prepared by hydrothermal techniques (14, 15) and have rationalized the results by interatomic potential calculations (15, 16). In the case of the tetravalent ions (14, 16) the main group Sn^{4+} ion and the transition metal Ti^{4+} ion give identical defect structures in which the dopants adopt two distinct sites: in addition to partially substituting at the octahedral sites, they also occupy the interstitial sites which are vacant in the α-Fe_2O_3 structure. However, to avoid the highly repulsive electrostatic interactions between M^{4+} and Fe^{3+} ions in linked face-sharing octahedra, the octahedral sites on both sides of the MO_6 units are vacant. In such a way, linear clusters of three M^{4+} ions replacing four Fe^{3+} ions occur to achieve charge balance while avoiding all face-sharing of MO_6 octahedra. In the case of divalent main group Mg^{2+} ions (15) the incorporation of Mg^{2+} is less influenced by such repulsive interactions and the divalent ions occupy the vacant interstitial sites as well as substituting on the two adjacent Fe^{3+} sites in the corundum-related α-Fe_2O_3 structure such that three Mg^{2+} ions replace two Fe^{3+} ions in a linear chain. In these materials Mg^{2+} behaves as an ionic divalent cation, adopting six-coordination to oxygen as might be expected. We have also shown (17, 18) that cation doping in α-Fe_2O_3 tends to reduce the magnitude of the hyperfine magnetic field and causes a decrease in the temperature of the Morin transition, T_M.

We have now extended out studies to the doping of a divalent transition metal, Zn^{2+}, into α-Fe_2O_3, where it is less likely that Zn^{2+} will act as a divalent metal cation adopting octahedral coordination. We report here on the structural characterization of Zn^{2+}-doped α-Fe_2O_3 by X-ray powder diffraction and X-ray absorption spectroscopy supported by interatomic potential calculations and on the effect of Zn^{2+} on the magnetic properties of α-Fe_2O_3 as revealed by ^{57}Fe Mössbauer spectroscopy.

EXPERIMENTAL

Zinc-doped α-Fe_2O_3 was prepared by precipitating aqueous mixtures of iron(III) chloride hexahydrate and zinc(II) chloride with aqueous ammonia and hydrothermally processing the suspension (*ca.* 250 ml) in a Teflon-lined autoclave at 200°C and 15 atm pressure for 6 h. The product was removed by filtration and washed with 95% ethanol until

[1] To whom correspondence should be addressed.

0022-4596/01 $35.00

no chloride ions were detected by silver nitrate solution. The product was dried at 140°C (12 h). The metal contents were determined by ICP and EDX analysis.

X-ray powder diffraction data were recorded with a Siemens D5000 diffractometer in reflection mode using Cu$K\alpha$ radiation.

Zinc K-edge extended X-ray absorption fine structure measurements were performed at the Synchrotron Radiation Source at Daresbury Laboratory (UK) with an average current of 200 mA at 2 GeV. The data were collected in fluorescence geometry on Station 16.5 at 298 K. The raw data were background-subtracted using the Daresbury program EXBACK and fitted using the nonlinear least squares minimization program EXCURV98, which calculates the theoretical EXAFS functions using the fast curved wave theory.

Interatomic potential calculations were performed using a pair potential shell model on a DEC alpha 600 workstation using the program GULP (19). The interatomic potentials for Fe^{3+} and O^{2-} were taken from a recently reported compilation (20). Those for Zn^{2+} were obtained by fitting to the structure of ZnO using the O^{2-} potential for α-Fe_2O_3.

The ^{57}Fe Mössbauer spectra were recorded in transmission geometry using a *ca.* 50 mCi ^{57}Co/Rh source with a multiscaler of 512 channels in constant acceleration mode. A Displex helium closed-cryogenic refrigerator operating in the range 18 to 300 K ($\pm$ 0.2 K) was used for the low temperature measurements. The ^{57}Fe Mössbauer spectra recorded *in situ* at elevated temperature were obtained with a constant acceleration spectrometer and a *ca.* 10 mCi ^{57}Co/Rh source using a furnace which has been described in detail elsewhere (21). All chemical isomer shift data are quoted relative to the centroid of the metallic iron spectrum at room temperature.

RESULTS AND DISCUSSION

The X-ray powder diffraction pattern recorded from the material, shown by EDX and ICP analysis to contain 4.32% Zn, showed the presence of an α-Fe_2O_3-related phase together with a small spinel-related $ZnFe_2O_4$ impurity (Fig. 1). Scanning electron microscopy indicated a particle size of ca. 100 nm. The presence of zinc within the α-Fe_2O_3 structure was confirmed by the ^{57}Fe Mössbauer spectrum recorded at 296 K (Fig. 2), which, as will be discussed in detail below, showed a sextet component characteristic of metal-doped corundum-related α-Fe_2O_3 (17, 18). The X-ray powder diffraction and analytical data show that the limit of solubility of Zn^{2+} in α-Fe_2O_3 is significantly lower than the ca. 6%, which was easily achieved in magnesium-doped α-Fe_2O_3 which we previously examined (15). Attempts to increase the zinc content in these materials were unsuccessful

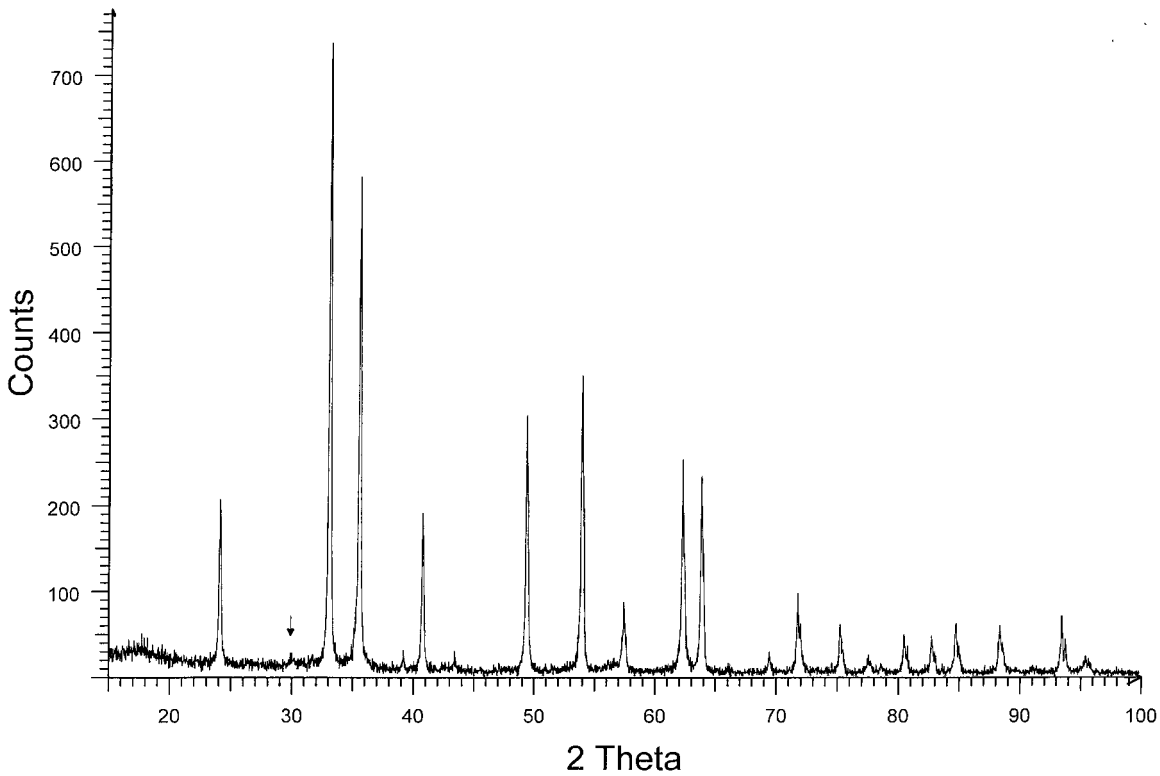

FIG. 1. X-ray powder diffraction pattern recorded from zinc-doped α-Fe_2O_3. The arrow indicates the $ZnFe_2O_4$ impurity phase.

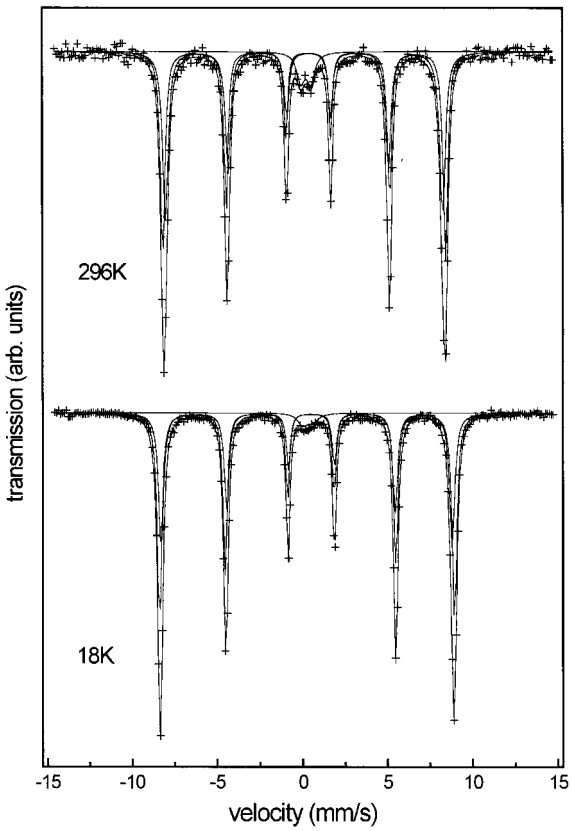

FIG. 2. ^{57}Fe Mössbauer spectra recorded from zinc-doped α-Fe_2O_3 at 296 and 18 K.

and we were unable to prepare monophasic samples of zinc-doped α-Fe_2O_3 with smaller amounts of zinc. The low zinc content precluded the refinement of X-ray- and neutron-powder diffraction data to a structural model. The small concentration of the $ZnFe_2O_4$ impurity phase precluded further characterization of this spinel-related material. The zinc K-edge EXAFS were also complicated by the biphasic nature of the sample. Given the analytical data and assuming that the recoil free fractions of iron in α-Fe_2O and $ZnFe_2O_4$ which contribute to the ^{57}Fe Mössbauer spectrum recorded at 296 K (see below) are equal we estimate that about two thirds of the zinc atoms are within the α-Fe_2O_3 structure, while the remainder are located within $ZnFe_2O_4$. Thus the zinc K-edge EXAFS (Fig. 3) were fitted to models in which two-thirds of the zinc atoms are located within α-Fe_2O_3 and the remainder occupy the octahedral sites of spinel-related $ZnFe_2O_4$. In the fitting procedure the Debye–Waller factors of the first and second oxygen shells and the iron atoms at similar distances in both α-Fe_2O_3 and $ZnFe_2O_4$ were constrained to be equal. Thus, 12 parameters were refined in fitting the data and enabled the successful fitting of the first and second oxygen shells and the first iron shell about zinc in zinc-doped α-Fe_2O_3 and $ZnFe_2O_4$. The zinc K-edge EXAFS for the zinc-doped α-Fe_2O_3 component were best fitted ($R = 34.16$) to a model for α-Fe_2O_3 (22) in which zinc substituted for iron on the cationic sublattice with an oxygen vacancy in the anionic sublattice and in coexistence with the $ZnFe_2O_4$ phase (Table 1). The fitting of further shells in both phases could not be performed with confidence.

Recognizing that the fitting of EXAFS data might not always be unequivocal in its interpretation and the need for supporting evidence for this model of Zn^{2+}-doped α-Fe_2O_3 which differs from that previously found for Mg^{2+}-doped α-Fe_2O_3 (15), we investigated a set of possible defect structures for the inclusion of Zn^{2+} in α-Fe_2O_3 through interatomic potential calculations using the program GULP (19) and according to methods which have previously been used for examining metal-doped α-Fe_2O_3 (15, 16). The same defect structures were investigated as in our earlier work involving Mg^{2+}-doped α-Fe_2O_3 (15). The potentials for

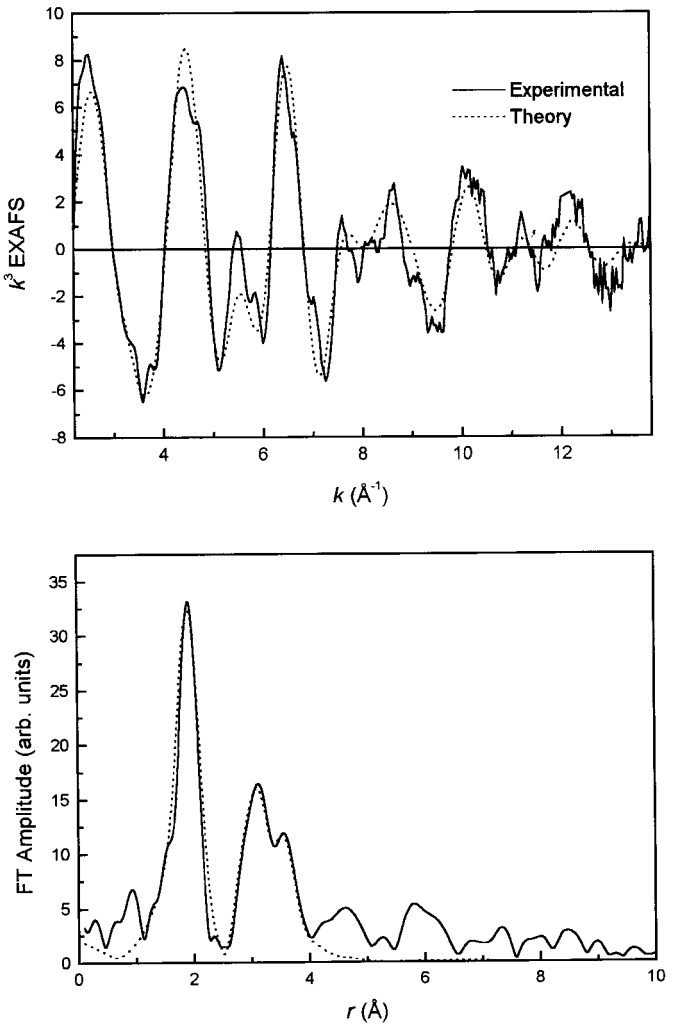

FIG. 3. Zinc K-edge EXAFS and Fourier transform recorded from zinc-doped α-Fe_2O_3. The experimental data are indicated by the solid line.

TABLE 1
Best Fit Parameters for Zinc K-Edge EXAFS Recorded from Zinc-Doped α-Fe_2O_3

Atom type	Coordination number	Distance (Å) ± 1%	$2\sigma^2$(Å^2)
Zn-doped α-Fe_2O_3			
O	5	1.97	0.019
Fe	4	2.97	0.021
Fe	3	3.37	0.027
O	6	3.22	0.016
$ZnFe_2O_4$			
O	4	1.97	0.019
Fe	12	3.49	0.027
O	12	3.52	0.016

α-Fe_2O_3 were the same as those used in our study of magnesium-doped α-Fe_2O_3 (15) which enables us to compare the effects of the two divalent ions. The best fit to ZnO using the oxygen potential for α-Fe_2O_3 was found using Buckingham parameters of $A = 400.87$ eV, $\rho = 0.3637$ Å, and a spring constant $k = 0.3445$ eV Å^{-2}. The core charge was -0.05. Lattice energies of -152.34 eV (α-Fe_2O_3) and -39.21 eV (ZnO) were used in the calculation. The calculated lattice parameters for ZnO were $a = 3.3466$ Å, $c = 4.965$ Å compared to the experimental $a = 3.2495$ Å, $c = 5.2069$ Å. The Buckingham A parameter was increased to 425.48 eV in the defect calculations to allow for the change in zinc from tetrahedral to octahedral coordination (23).

The defect structures investigated are described below using the Kröger–Vink notation.

(a) Replacement of Fe^{3+} ions by Zn^{2+} ions balanced by vacancies on half as many O^{2-} sites:

$$ZnO(s) + Fe_{Fe}^{\times} + \tfrac{1}{2}O_o^{\times} \rightarrow Zn'_{Fe} + \tfrac{1}{2}V_o^{\cdot\cdot} + \tfrac{1}{2}\alpha\text{-}Fe_2O_3(s).$$

(b) As (a) but with the zinc ions adjacent to the oxygen vacancies:

$$ZnO(s) + Fe_{Fe}^{\times} + \tfrac{1}{2}O_o^{\times} \rightarrow \tfrac{1}{2}(2Zn'_{Fe}V_o^{\cdot\cdot}) + \tfrac{1}{2}\alpha\text{-}Fe_2O_3(s).$$

(c) Occupation by Zn^{2+} ions of interstitial sites balanced by two-thirds the number of vacancies on Fe^{3+} sites:

$$ZnO(s) + \tfrac{2}{3}Fe_{Fe}^{\times} \rightarrow Zn_i^{\cdot\cdot} + \tfrac{2}{3}V'''_{Fe} + \tfrac{1}{3}\alpha\text{-}Fe_2O_3(s).$$

(d) As (c) but with the interstitial Zn^{2+} ions in sites adjacent to the vacancy:

$$ZnO(s) + \tfrac{2}{3}Fe_{Fe}^{\times} \rightarrow \tfrac{1}{3}(3Zn_i 2V'''_{Fe}) + \tfrac{1}{3}\alpha\text{-}Fe_2O_3(s).$$

(e) Occupation by Zn^{2+} of an interstitial site balanced by two vacancies on each of Fe^{3+} sites and O^{2-} sites:

$$ZnO(s) + 2Fe_{Fe}^{\times} + 2O_o^{\times} \rightarrow Zn_i^{\cdot\cdot} + 2V'''_{Fe} + 2V_o^{\cdot\cdot} + \alpha\text{-}Fe_2O_3(s)$$

(f) As (e) but with the vacancies adjacent to the interstitial ion:

$$ZnO(s) + 2Fe_{Fe}^{\times} + 2O_o^{\times} \rightarrow (Zn_i^{\cdot\cdot}2V'''_{Fe}2V_o^{\cdot\cdot}) + \alpha\text{-}Fe_2O_3(s).$$

(g) Substitution of Fe^{3+} by Zn^{2+} on two sites and occupation by Zn^{2+} of an interstitial site:

$$ZnO(s) + \tfrac{2}{3}Fe_{Fe}^{\times} \rightarrow \tfrac{1}{3}Zn_i^{\cdot\cdot} + \tfrac{2}{3}Zn'_{Fe} + \tfrac{1}{3}\alpha\text{-}Fe_2O_3(s).$$

(h) As (g) but with the two substituted sites flanking the interstitial site:

$$ZnO(s) + \tfrac{2}{3}Fe_{Fe}^{\times} \rightarrow \tfrac{1}{3}(Zn_i^{\cdot\cdot}2Zn'_{Fe}) + \tfrac{1}{3}\alpha\text{-}Fe_2O_3(s).$$

The results of these calculation are given in Table 2.

From these results, we predict that substitution for Fe^{3+} by Zn^{2+} would be more favorable than occupation of interstitial sites, see results for models a and c. A set of two isolated substituted zinc ions and a separate interstitial zinc ion was less favorable (model g). The clustering of defects considerably improved the defect energy. However, the cluster of two substituted and one interstitial zinc ions arranged as found for the most favorable defect cluster for magnesium-doped α-Fe_2O_3 (model h) (15) was less favorable than a cluster of two substituted ions adjacent to an oxygen vacancy (model b). Further evidence against the cluster as found for magnesium-doped α-Fe_2O_3 came from the failure to find an energy minimum for a supercell with this defect in the case of zinc-doped α-Fe_2O_3. This contrasts with the case for magnesium-doped α-Fe_2O_3 where the supercell successfully optimised with minimum energy. Our conclusion therefore, based on the best fit to the zinc K-edge EXAFS data and the interatomic potential calculations, is that zinc

TABLE 2
Defect Energies for Zn^{2+} Doped into α-Fe_2O_3

Model	Defect energy per mol Zn^{2+} (eV)
a	3.21
b	0.77
c	9.68
d	1.77
e	20.60
f	5.63
g	3.55
h	1.08

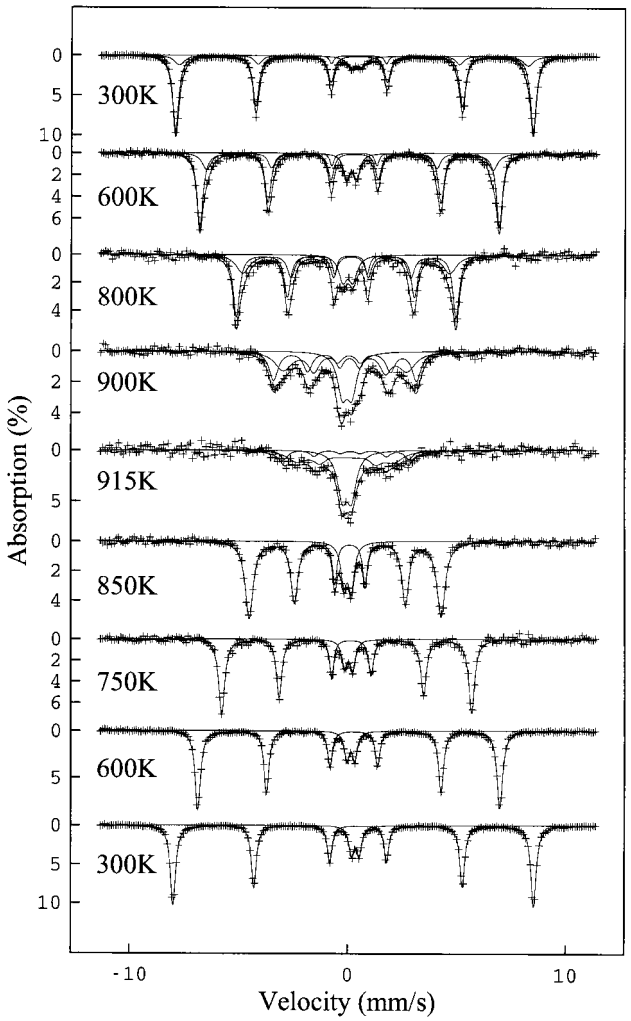

FIG. 4. ^{57}Fe Mössbauer spectra recorded *in situ* from zinc-doped α-Fe_2O_3 on heating between 300 and 915 K and on subsequent cooling to 300 K.

ions substitute for Fe^{3+} ions and are accompanied by oxygen vacancies.

The ^{57}Fe Mössbauer spectrum recorded at 296 K (Fig. 2) showed the superposition of a sextet pattern and a broad doublet. The doublet component, $\delta = 0.34\ \text{mm s}^{-1}$, $\Delta = 0.54\ \text{mm s}^{-1}$ at 296 K, $\delta = 0.44\ \text{mm s}^{-1}$, $\Delta = 0.54\ \text{mm s}^{-1}$ at 18 K, is characteristic of the $ZnFe_2O_4$ impurity phase (24, 25) and remained constant (*ca.* 6%) in all spectra recorded at temperatures between 296 and 18 K (Fig. 2). The fitting of the magnetically split component of the spectrum to a single sextet gave a hyperfine magnetic field H of 51.2 ± 0.3 T, which is smaller than that of pure α-Fe_2O_3. However, the linewidth ($0.32\ \text{mm s}^{-1}$) is indicative of a distribution of sites originating from the presence of the dopant zinc within the α-Fe_2O_3 structure. The spectrum was therefore fitted to two sextet patterns. The pattern with the larger field ($H_1 = 51.5 \pm 0.3$ T) can be associated with Fe^{3+} ions which are not influenced by the presence of zinc, while that with the smaller field ($H_2 = 50.5 \pm 0.3$ T) can be assigned to Fe^{3+} ions that have Zn^{2+} ions in close proximity. The relative population of each magnetic component varied with assumed linewidth without any significant change to the value of χ^2 and the percentage of Fe^{3+} influenced by zinc is therefore difficult to quantify. However, by constraining the minimum linewidths to the calibration value ($0.25\ \text{mm s}^{-1}$), relative proportions of 52 ± 2 and $42 \pm 4\%$ for H_1 and H_2 were obtained.

The spectrum recorded at 18 K (Fig. 3) demonstrated that the Morin transition in α-Fe_2O_3 is completely suppressed by the presence of zinc. Indeed, the negative values of the quadrupole coupling constants for both magnetic components ($2\varepsilon = -0.22$ and $-0.24\ \text{mm s}^{-1}$) indicate that the material is weakly ferromagnetic at low temperatures.

The ^{57}Fe Mössbauer spectra recorded *in situ* from zinc-doped α-Fe_2O_3 while increasing the temperature from 300 to 915 K and subsequently decreasing the temperature from 915 to 300 K are shown in Fig. 4. The ^{57}Fe Mössbauer parameters for the spectra recorded at 300 and 600 K before and after heating are collated in Table 3. All the spectra were recorded over 48 h at the specified temperature except that recorded at 915 K, which was recorded over 8 h. The first three spectra recorded at 300, 600, and 800 K were best fitted to two sextet patterns, characterising the hyperfine magnetic field distribution resulting from the introduction of zinc into the corundum-related α-Fe_2O_3 structure, and a broad-line doublet with Mössbauer parameters similar to those previously reported for $ZnFe_2O_4$ (24, 25). The variation of the hyperfine magnetic field with temperature, $B(T)$ (Fig. 5), closely followed the curve previously observed for magnesium-doped α-Fe_2O_3 (18) and lies approximately 0.6 T below the field obtained from pure α-Fe_2O_3. The spectra recorded at 900 and 915 K were less amenable to fitting to three components as a result of the transformation of the magnetically ordered smaller particles to superparamagnetic α-Fe_2O_3 and also the conversion of zinc-doped α-Fe_2O_3 to spinel-related $ZnFe_2O_4$. This is different from the results obtained from magnesium-doped α-Fe_2O_3 (18), where no evidence for the formation of a spinel structure at elevated temperature was observed. In the case of magnesium-doped α-Fe_2O_3 the variation of the hyperfine magnetic field with temperature $B(T)$ showed no hysteresis between the hyperfine magnetic fields obtained from spectra in the heating and cooling regimes. In the case of zinc-doped α-Fe_2O_3 there is hysteresis of *ca.* 0.6 T. The spectra recorded *in situ* as the temperature was reduced were best fitted to one sextet of narrow linewidth $< 0.30\ \text{mm s}^{-1}$, accounting for *ca.* 86% of the area, and with hyperfine parameters (Table 3) typical of those of pure α-Fe_2O_3 and a doublet with an isomer shift following the same second order Doppler shift as that observed during the heating regime. The doublet is characterized by narrow linewidths ($0.28\ \text{mm s}^{-1}$)

TABLE 3
^{57}Fe Mössbauer Parameters for Zinc-Doped α-Fe_2O_3

Temperature (K)	$\delta \pm 0.01$ (mm/s)	$\Delta \pm 0.01$ (mm/s)	T $\pm$ 0.3 (Tesla)	Peak area ratio %
Before annealing at 900 K				
300 Sextet 1	0.37	− 0.21	50.9	75
Sextet 2	0.35	− 0.23	49.6	16
Doublet	0.34	0.47		8
600 Sextet 1	0.16	− 0.22	42.6	65
Sextet 2	0.16	− 0.21	40.8	24
Doublet	0.13	0.46		11
After annealing at 900 K				
600 Sextet	0.16	− 0.22	43.0	86
Doublet	0.13	0.36		14
300 Sextet	0.37	− 0.22	51.6	86
Doublet	0.36	0.35		14

and a quadrupole splitting of 0.35 mm s^{-1} identical to that for $ZnFe_2O_4$ (24, 25). The observation at 300 K of a sextet pattern with hyperfine parameters characteristic of pure α-Fe_2O_3 and a doublet typical of $ZnFe_2O_4$ suggest that at the elevated temperatures all the zinc in the α-Fe_2O_3 phase is converted to spinel-related $ZnFe_2O_4$.

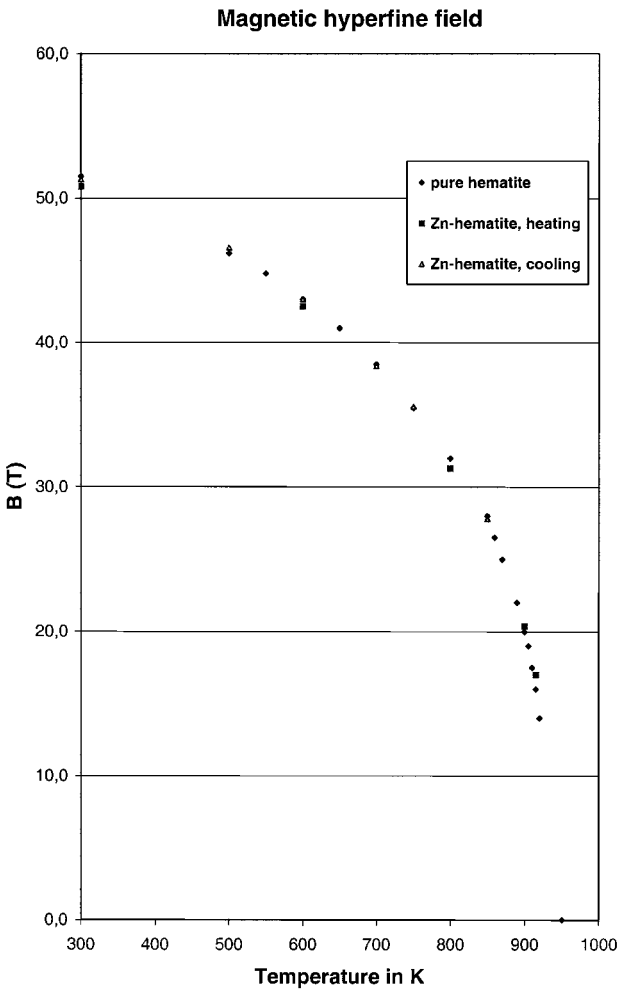

FIG. 5. Variation of hyperfine magnetic field with temperature for zinc-doped α-Fe_2O_3 and α-Fe_2O_3.

CONCLUSIONS

The limit of solubility of Zn^{2+} within the corundum-related α-Fe_2O_3 structure (*ca.* 2.88%) is significantly less than the solubility limit of *ca.* 6% of Mg^{2+} which can be accommodated within α-Fe_2O_3. Zinc K-edge EXAFS and interatomic potential calculations indicate that Zn^{2+} ions substitute for Fe^{3+} ions in the lattice and are accompanied by oxygen vacancies. This defect structure is different from that observed in Mg^{2+}-doped α-Fe_2O_3. The ^{57}Fe Mössbauer spectra show that the Morin transition is completely suppressed by the presence of zinc in α-Fe_2O_3. At elevated temperatures Zn^{2+}-doped α-Fe_2O_3 is converted to spinel-related $ZnFe_2O_4$, a result which contrasts with the thermal stability of Mg^{2+}-doped α-Fe_2O_3 at similar temperatures.

ACKNOWLEDGMENTS

R.C.M. is a member of CONICET who we thank for the award of a Postdoctoral Fellowship (S.J.S.). We thank the EPSRC for the award of beam time at Daresbury Laboratory.

REFERENCES

1. F. J. Morin, *Phys. Rev.* **83,** 1005 (1951).
2. N. Uekawa, M. Watanabe, K. Kaneko, and F. Mizukami, *J. Chem. Soc. Faraday Trans.* **91,** 2161 (1995).
3. P. B. Fabritchnyi, E. V. Lamykin, A. M. Babechkin, and A. N. Nesmeianov, *Solid State Commun.* **11,** 343 (1972).
4. F. Schneider, K. Melzer, M. Mehner, and G. Deke, *Phys. Status Solidi.* (a) **39,** K115 (1977).
5. M. Takano, Y. Bando, N. Nakanishi, M. Sakai, and H. Okinaka, *J. Solid State Chem.* **68,** 153 (1987).
6. S. Music, S. Popovic, M. Metikos-Hukovic, and E. Gvozdic, *J. Mater. Sci. Lett.* **10,** 197 (1991).

7. H. Kanai, H. Mizutani, T. Tanaka, T. Funabiki, S. Yoshida, and M. Takano, *J. Mater. Chem.* **2,** 703 (1992).
8. E. De Grave, D. Chambaere, and L. H. Bowen, *J. Magn. Magn. Mater.* **30,** 349 (1983).
9. E. De Grave, L. M. Bowen, and S. B. Weed, *J. Magn. Magn. Mater.* **27,** 98 (1982).
10. S. A. Fysh and P. E. Clark, *Phys. Chem. Miner.* **8,** 257 (1982).
11. S. Music, S. Popovic, and M. Ristic, *J. Mater. Sci.* **24,** 2722 (1989).
12. M. Ristic, S. Popovic, M. Tonkovic, and S. Music, *J. Mater. Sci.* **26,** 4225 (1991).
13. M.-Z. Dang, D. G. Rancourt, J. E. Dutrizac, G. Lamarche, and R. Provencher, *Hyperfine Interact.* **117,** 271 (1998).
14. F. J. Berry, C. Greaves, J. McManus, M. Mortimer, and G. Oates, *J. Solid State Chem.* **130,** 272 (1997).
15. F. J. Berry, A. Bohorquez, C. Greaves, J. McManus, E. A. Moore, and M. Mortimer, *J. Solid State Chem.* **140,** 428 (1998).
16. F. J. Berry, A. Bohorquez, and E. A. Moore, *Solid State Commun.* **109,** 207 (1999).
17. F. J. Berry, C. Greaves, Ö. Helgason, K. Jónsson, J. McManus, and S. J. Skinner, *in* "Mössbauer Spectroscopy in Materials Science" (M. Miglierini and D. Petrides, Eds.), NATO Science Series, p. 1. Kluwer, Dordrecht, 1999.
18. F. J. Berry, C. Greaves, Ö. Helgason, J. McManus, H. M. Palmer, and R. Williams, *J. Solid State Chem.* **151,** 157 (2000).
19. J. D. Gale, *J. Chem. Soc. Faraday Trans.* **93,** 629 (1997). J. D. Gale, "General Utility Lattice Program (GULP)" 1992–1994, London, The Royal Institution and Imperial College.
20. T. S. Bush, J. D. Gale, C. R. A. Catlow, and P. D. Battle, *J. Mater. Chem.* **4,** 831 (1994).
21. O. Helgason, H. P. Gunnlausson, K. Jónsson, and S. Steinthorsson, *Hyperfine Interact.* **9,** 595 (1994).
22. A. Manceau and J. M. Combes, *Phys. Chem. Mineral.* **15,** 283 (1988).
23. G. V. Lewis and C. R. A. Catlow, *J. Phys. C* **18,** 1149 (1985).
24. T. Mizoguchi and M. Tanaka, *J. Phys. Soc. Jpn.* **18,** 1301 (1963).
25. A. Hudson and H. J. Whitfield, *Mol. Phys.* **12,** 165 (1967).